

3. I. M. Basset, M. A. Box, R. G. Hewitt, *Search* 5 (no. 5), 182 (1974).
4. R. T. Watson and Ozone Trends Panel, M. J. Prather and Ad Hoc Theory Panel, and M. J. Kurylo and NASA Panel for Data Evaluation, "Present state of knowledge of the upper atmosphere 1988: An assessment report" [NASA RP-1208, National Aeronautics and Space Administration (NASA) Office of Space Science and Application, Washington, DC, 1988].
5. M. J. Prather, M. B. McElroy, S. C. Wofsy, *Nature* 312, 227 (1984); World Meteorological Organization, *Atmospheric Ozone 1985, Assessment of Our Understanding of the Process Controlling Its Present Distribution and Change* (NASA, Washington, DC, 1986); R. T. Watson, M. A. Geller, R. S. Stolarski, R. F. Hampson, *NASA RP-1162* (1986); L. B. Callis and M. Natarajan, *Nature* 323, 772 (1986); J. C. Farman, B. G. Gardiner, J. D. Shanklin, *ibid.* 315, 207 (1985); S. Solomon, R. R. Garcia, F. S. Rowland, D. J. Wuebbles, *ibid.* 321, 755 (1986).
6. J. Scotto, G. Cotton, F. Urbach, D. Berger, T. Fears, *Science* 239, 762 (1988).
7. D. S. Berger and F. Urbach, *Photochem. Photobiol.* 35, 187 (1982).
8. D. S. Berger, in *Human Exposure to Ultraviolet Radiation: Risks and Regulations*, W. F. Passchier and B. F. M. Bosnjakovic, Eds. (Elsevier, New York, 1987), pp. 213–221.
9. N. Robinson, *Solar Radiation* (Elsevier, New York, 1966), p. 114.
10. M. Blumthaler and W. Ambach, *Atmos. Environ.* 22, 749 (1988).
11. H. Canaval, *Photochem. Photobiol.* 42, 147 (1985).
12. D. S. Berger, *ibid.* 24, 587 (1976).
13. B. L. Diffey, *ibid.* 46, 55 (1987).
14. D. H. Sliney, *Am. Ind. Hyg. Assoc. J.* 33, 644 (1972).
15. J. DeLuigi and J. Harris, *Atmos. Environ.* 17, 751 (1983).
16. M. Blumthaler and W. Ambach, *Arch. Meteorol. Geophys. Bioklimatol. Ser. B* 36, 357 (1986).
17. J. Stachelin and H. Dütsch, *Chimia* 43, 338 (1989).
18. J. Slomka, *Publ. Inst. Geophys. Pol. Acad. Sci. D* 30 (220), 163 (1988).
19. H. T. Mantis, C. S. Zerefos, A. Bais, I. Ziomas, A. Kelesis, *Arch. Meteorol. Geophys. Bioklimatol. Ser. B* 36, 135 (1986).
20. J. K. Angell, J. Korshover, W. G. Planet, *Mon. Weather Rev.* 113, 641 (1985).
21. We thank the head of the High Alpine Research Station Jungfraujoch, Bern, for assistance. Supported by the Austrian Academy of Sciences, Vienna.

12 October 1989; accepted 8 February 1990

Phosphate-Methylated DNA Aimed at HIV-1 RNA Loops and Integrated DNA Inhibits Viral Infectivity

HENK M. BUCK, LEO H. KOOLE, MARCEL H. P. VAN GENDEREN, LIA SMIT, JAN L. M. C. GEELLEN, SUZANNE JURRIAANS, JAAP GOUDSMIT

Phosphate-methylated DNA hybridizes strongly and specifically to natural DNA and RNA. Hybridization to single-stranded and double-stranded DNA leads to site-selective blocking of replication and transcription. Phosphate-methylated DNA was used to interrupt the life cycle of the human immunodeficiency virus type-1 (HIV-1), the causative agent of acquired immunodeficiency syndrome (AIDS). Both antisense and sense phosphate-methylated DNA 20-nucleotide oligomers, targeted at the transactivator responsive region and the primer binding site, caused complete inhibition of viral infectivity at a low concentration. Hybridization of phosphate-methylated DNA with folded and unfolded RNA was studied by ultraviolet and proton nuclear magnetic resonance spectroscopy. The combined results of hybridization studies and biological experiments suggest that the design of effective antisense phosphate-methylated DNA should focus on hairpin loop structures in the viral RNA. For sense systems, the 5' end of the integrated viral genome is considered to be the important target site.

IT HAS BEEN SHOWN THAT PHOSPHORothioate, phosphoramidate, and methyl phosphonate oligodeoxynucleotides are potential antiviral agents because their specific hybridization to viral sequences leads to inhibition of replication and gene expression, and because they are very resistant to cellular exo- and endonucleases (1–3). In principle, neutrally charged backbones will lead to strong hybridization (as a conse-

quence of the absence of interstrand phosphate-phosphate charge repulsions), stability toward nucleases, and facile transport through cell membranes (4). Phosphate-methylated DNA shows particular promise in that this neutral modification exhibits the best conformational accommodation to natural DNA and RNA (5–7) (Fig. 1A).

Our initial experiments on the strength of hybridization of phosphate-methylated DNA with natural single-stranded DNA are shown in Fig. 1B. Hybridization of phosphate-methylated d(GGA.ATC.CTG.CAG) with its natural complement shows a transition temperature (T_m) of 55°C, whereas the corresponding natural duplex does not exist in salt-free solution. Addition of 0.1M

NaCl, which diminishes interstrand phosphate-phosphate charge repulsions since the Na^+ ions tend to neutralize the negative phosphate charges, results in a T_m of 42°C for the natural duplex and represents a physiological salt solution. For hybridization with unfolded RNA, we studied the duplex formation of phosphate-methylated d(C_n) ($n = 3, 5, 10, \text{ and } 20$) with poly(rG) (8). The T_m values were 13°, 28°, 36°, and 51°C, respectively. For comparison, natural d(C_n) ($n = 3, 5, 10, \text{ and } 20$) did not associate with poly(rG) under the condition of 0.1M NaCl. Phosphate-methylated DNA–natural DNA duplexes are more stable than phosphate-methylated DNA–RNA duplexes

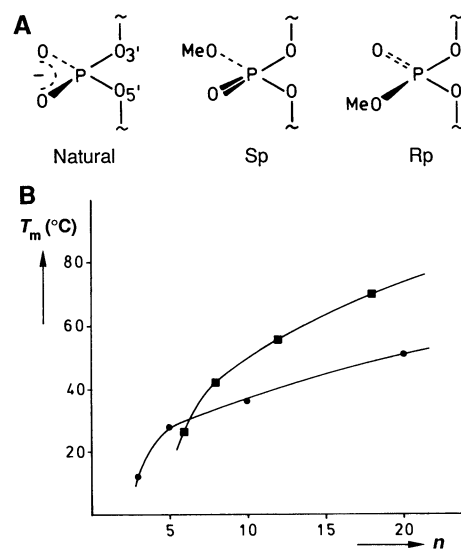


Fig. 1. (A) Structural formulas of natural phosphate, and S_p and R_p methyl phosphotriester groups. Investigations on the dinucleotide systems d(TpT), d(ApT), d(ApC), d(ApA), d(GpC), d(CpC), and d(TpC) with 600-MHz proton NMR spectroscopy (5) revealed that the diastereoisomeric phosphate-methylated forms possess virtually identical conformational features in aqueous solution, which closely resemble a right-handed B helix structure (27), namely C_2' -endo puckered sugar rings: R_p 59%, S_p 60%, and natural 61%; $\gamma^+(C_4'-C_5'$ backbone bond): R_p 63%, S_p 57%, and natural 59%; $\beta^+(C_5'-O_5'$ bond): R_p 66%, S_p 69%, and natural 84% (percentages denote time-averaged contribution of these conformations). R_p , S_p , and natural systems show anti orientation of the bases. (B) Duplex \rightleftharpoons coil T_m 's for hybrids of phosphate-methylated DNA oligomers of length n , with complementary natural DNA (\blacksquare) and RNA (\bullet), as determined with ultraviolet (UV) hyperchromicity. The total nucleotide concentration in all experiments was 2 μM . T_m values were independent of the ionic strength of the solution, which was consistent with the absence of interstrand phosphate-phosphate charge repulsions. Melting transitions occurred within 10°C intervals, implying that hybridization was equally strong for all diastereoisomeric forms (28). The duplexes of phosphate-methylated d(GGA.ATC), d(AGC.CTG.AC) and d(CAC.TCA.CCC.ATG.AAC.AGC) with their natural complements displayed T_m values of 27°, 42°, and 70°C, respectively (6).

H. M. Buck, L. H. Koole, M. H. P. van Genderen, Department of Organic Chemistry, Eindhoven University of Technology, P.O. Box 513, 5600 MB Eindhoven, The Netherlands.
L. Smit, J. L. M. C. Geelen, S. Jurriaans, J. Goudsmit, Human Retrovirus Laboratory, AMC, Department of Virology, Meibergdreef 15, 1105 AZ Amsterdam, The Netherlands.

(Fig. 1B) despite the presence of only G-C base pairs in the latter case. We suggest the difference in stability is due to the structural match between phosphate-methylated and natural DNA, which both adopt the B-geometry, whereas RNA has the A structure (9). Region-specific hybridization of a phosphate-methylated 18-nucleotide oligomer with single-stranded DNA, inserted in an M13mp18 phage, was found to block replication of the template at the selected site (6). Hybridization in which the target was cellular duplex DNA resulted in inhibition of transcription (10).

Our primary work concerns the hybridization of phosphate-methylated DNA with HIV-1-specific RNA. To mimic the folded structure in viral RNA, we performed experiments with yeast phenylalanine transfer RNA ($tRNA^{Phe}$), which has a well-defined molecular conformation (11). A phosphate-methylated 18-nucleotide oligomer was targeted at the amino acid stem and the T Ψ C arm, encompassing six free bases (four dangling bases at the 3' end and two bases in the T Ψ C hairpin loop) (Fig. 2A). High-field proton nuclear magnetic resonance (NMR) experiments revealed that the phosphate-methylated 18-nucleotide oligomer hybridized over its full length with $tRNA^{Phe}$; hybridization was accompanied by unfolding of the amino acid stem and the T Ψ C arm, with preservation of the anticodon and D arms (Fig. 2B). This information was used to select four 20-nucleotide target sites in HIV-1 RNA on the basis of the secondary structure as calculated with Zuker and Stiegler's FOLD program (12) (Fig. 3).

Strong inhibition of syncytium formation in HIV-1-infected cells was found for two antisense phosphate-methylated 20-nucleotide oligomers (13), namely the TAR construct (complementary to a site in the transactivator-responsive region), and the PBS construct (complementary to a site adjacent to the primer binding site) (Table 1). The inhibitory concentration for the HX10 clone of HTLV-III_B at a virus titer of 1000 median tissue culture infectious doses (TCID₅₀) was 0.3 μ M for TAR and PBS, whereas the NEF and VIF 20-nucleotide oligomer constructs (complementary to the transcription initiation sites of the *nef* and *vif* genes) were found to be substantially less active (inhibitory concentrations 3 μ M for NEF and 15 μ M for VIF). The corresponding natural antisense 20-nucleotide oligomers were found to be inactive up to concentrations of 3 to 15 μ M.

On the basis of the virtual absence of all viral DNA (AVD, which includes circular and linear unintegrated DNA, and integrated DNA), circular unintegrated viral DNA (cUVD) specifically, and viral p24 core pro-

tein, it was concluded that antisense phosphate-methylated DNA blocks the reverse transcription of viral RNA (13) (Table 1). Data indicate that the inhibitory effect of antisense phosphate-methylated DNA is strongly influenced by the secondary structure of the target region in the viral RNA. We suggest that the hairpin loop in the TAR and PBS sites assists in the hybridization

with phosphate-methylated DNA (14). Data concerning hybridization-induced antiviral activity of phosphorothioate, phosphoramidate, and methyl phosphonate DNA with other target sites strengthen the predictive value of this structure-activity relation (15-18). The inhibitory concentrations for the antisense phosphate-methylated TAR and PBS constructs are very low compared to

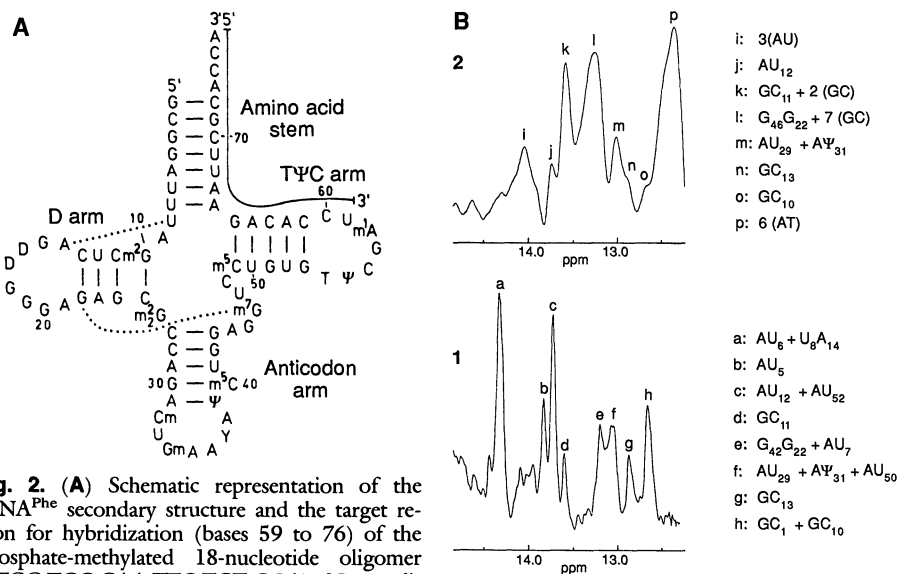


Fig. 2. (A) Schematic representation of the $tRNA^{Phe}$ secondary structure and the target region for hybridization (bases 59 to 76) of the phosphate-methylated 18-nucleotide oligomer d(TGG.TGC.GAA.TTC.TGT.GGA). No modified nucleotides are present in the target site. Relevant tertiary hydrogen bonds are present in the target site. (B) Part of the imino-proton region of the 400-MHz proton NMR spectra at 20°C of $tRNA^{Phe}$ (spectrum 1), and of an equimolar mixture of $tRNA^{Phe}$ and phosphate-methylated 18-nucleotide oligomer (spectrum 2). Imino resonances are found in the case of base pairing; in unpaired bases, imino resonances disappear because of rapid exchange with the solvent. All measurements were performed in salt-free H₂O/D₂O mixtures (90:10) at pH 7; concentrations of $tRNA^{Phe}$ and phosphate-methylated 18-nucleotide oligomer amounted to 2 mM. The mixture was measured without annealing at elevated temperatures. The water peak (4.68 ppm) was suppressed by combined application of a semi-selective observation pulse and digital shift accumulation (29). Curve-fitting was performed in order to determine peak areas. Assignments in spectrum 1 (peaks a to h) were as in (30). Spectrum 2 (peaks i to p) indicates dissociation of the amino acid stem and the T Ψ C arm due to hybridization with phosphate-methylated 18-nucleotide oligomer, and preservation of the anticodon and D arms. Unfolding of the amino acid stem is evident from the disappearance of the AU₆ + U₈A₁₄ (a) and AU₅ (b) imino resonances. The D arm is conserved, as is seen from the presence of the GC₁₃ (n) imino resonance in both spectra (g and n). Both observations are consistent with the fact that the GC₁ + GC₁₀ signal (h) leads to a single-proton signal (o) caused by the remaining GC₁₀ base pair. The T Ψ C arm is dissociated, as is concluded from the AU₁₂ + AU₅₂ signal (c), which results in a single-proton signal (j), corresponding to the AU₁₂ base pair in the D arm. Preservation of the anticodon arm follows from AU₂₉ + A Ψ ₃₁ + AU₅₀ signal (f). A two-proton signal remains (m), that is, the AU₂₉ and A Ψ ₃₁ base pairs in the anticodon arm are intact. New imino resonances (indicated in brackets) arise from the hybridization of the amino acid stem and the T Ψ C arm with phosphate-methylated 18-nucleotide oligomer, involving nine G-C (k and l), six A-T (p), and three A-U (i) base pairs. The assignment of the G-C base pairs to k and l is based on the fact that the imino protons in the duplex of phosphate-methylated d(C₂₀) and poly(rG) (Fig. 1B) resonate at 13.4 ppm. Assignment of the A-T and A-U base pairs is based on the peak areas of p and i, which correspond to six and three protons, respectively. The reversible dissociation of the phosphate-methylated DNA- $tRNA^{Phe}$ hybrid was studied with variable-temperature NMR and UV hyperchromicity. At a sample temperature of 50°C, no imino resonances are seen for $tRNA^{Phe}$, whereas the mixture of $tRNA^{Phe}$ and phosphate-methylated 18-nucleotide oligomer after heating to 50°C showed imino resonances at 12.8, 13.4, and 13.9 ppm (peak areas 6:9:3), that is, these signals result from the duplex of phosphate-methylated DNA with bases 59 to 76 of $tRNA^{Phe}$. The central signal is assigned to the G-C base pairs, based on the imino-proton location at 13.5 ppm in the duplex of phosphate-methylated d(C₂₀) and poly(rG) at 50°C. The A-T and A-U base pairs correspond to the signals at 13.9 and 12.8 ppm, respectively, as is seen from the peak areas. Further increase of the sample temperature to 60°C results in disappearance of all imino resonances, indicating a T_m of ~55°C for the phosphate-methylated DNA- $tRNA^{Phe}$ duplex at 2 mM concentration. In a UV hyperchromicity experiment at 2 μ M concentration, the T_m was found at 44°C, which is slightly lower than expected from the experiments with unfolded RNA (Fig. 1B) because the G-C content is now only 50%. For the mixture of phosphate-methylated 18-nucleotide oligomer and $tRNA^{Phe}$, no T_m was obtained for the D and anticodon arms in the UV measurement. This is in agreement with a control experiment, which showed that all four arms of $tRNA^{Phe}$ dissociate at 27°C for concentrations of 2 μ M.

previous results concerning inhibition of HIV-1 with other types of modified DNAs (phosphorothioates, phosphoramidates, or methyl phosphonates) for which inhibitory concentrations of 3 to 15 μM are required at a virus titer similar to that used in our experiments (16, 17).

Because of the high inhibitory activity of the antisense phosphate-methylated systems, we also studied inhibition of syncytium formation with the sense phosphate-methylated 20-nucleotide oligomers (13), namely, the TAR, PBS, NEF, and VIF constructs. These systems block transcription of integrated proviral DNA as measured by the absence of viral p24 core protein, whereas formation of viral DNA (cUVD and AVD) could be clearly established (13) (Table 1). Similar inhibitory concentrations for 1000 TCID₅₀ of the HX10 clone of HTLV-III_B were found in comparison with the antisense systems. Therefore, we concluded that hybridization arrest is most effective at the start of the transcription, which is just upstream of the TAR and PBS target regions. The results also show inhibition of HIV-1 after integration, which is especially relevant for chronically infected cells (19).

The sequence-specificity of the inhibition by phosphate-methylated DNA was investigated by testing the antisense and sense TAR and PBS constructs, as well as the random system (RAN; Fig. 3A), on cells infected with the HIV-1 variants HTLV-III_{RF} and RUT. In HTLV-III_{RF}, one muta-

Table 1. Inhibition of viral infectivity by phosphate-methylated DNA. H9 cells were grown in RPMI 1640 (Gibco), 10% fetal calf serum, 2 mM glutamine, and antibiotics. Virus stocks were prepared by mixing 3.2×10^6 uninfected H9 cells with 0.8×10^6 infected H9 cells in 20 ml of culture medium (48 hours at 37°C); extracellular virus was harvested by centrifugation (1000g for 10 min), then filtered through a 0.22- μm filter (Millipore SA), and stored at -196°C. Infectious titers were determined by end-point titration on C81-66 cells. Inhibition of HIV-1 infectivity on C81-66 cells in the presence of oligodeoxynucleotides was tested by infecting 2×10^4 cells per 100 μl of medium with 40 μl of virus dilution, containing 1000 TCID₅₀. Each concentration of oligodeoxynucleotide was tested in quadruplicate. Experiments were reproducible at various times for all constructs. The plates were incubated (37°C for 5 days), and the lowest concentration without syncytia was taken as the inhibitory concentration. For measurements of p24, cUVD, and AVD infected cells were exposed to oligodeoxynucleotides (3 μM) for 5 days, and the supernatant and cells were separately heat-inactivated (56°C for 30 min). HIV-1 p24 expression was measured in the supernatant with a solid-phase immunoassay (Abbott Labs) (25). For detection of cUVD and AVD, total DNA was extracted from the inactivated cells, and 10 to 50 ng was used in the polymerase chain reaction (26).

| Virus strain | Construct* | Inhibitory concentration† (μM) | p24 (pg/ml) | cUVD‡ | AVD‡ |
|-----------------------|------------------------|---|-------------|-------|------|
| HTLV-III _B | (-)TAR | 0.3 | 496 | - | + |
| | (+)TAR | 0.6 | 532 | + | ++ |
| | nat(-)TAR | >3.0 | >10,000 | ++ | ++ |
| | (-)PBS | 0.3 | | | |
| | (+)PBS | 0.3-0.6 | | | |
| | nat(-)PBS | >3.0 | | | |
| | (-)NEF | 3.0 | | | |
| | (+)NEF | >15.0 | | | |
| | nat(-)NEF | >3.0 | | | |
| | (-)VIF | 15.0 | | | |
| | (+)VIF | 3.0-15.0 | | | |
| | nat(-)VIF | >15.0 | | | |
| | HTLV-III _{RF} | (-)TAR | 3.0 | 200 | - |
| (+)TAR | | 3.0 | 160 | - | + |
| (-)PBS | | 0.15-0.3 | | | |
| (+)PBS | | 0.6 | | | |
| RUT | (-)TAR | >6.0 | >10,000 | + | + |
| | (+)TAR | >6.0 | >10,000 | + | + |

*Nat, natural, nonphosphate methylated form. †Inhibitory concentrations refer to the HX10 clone of HTLV-III_B. ‡+ and ++ indicate relative intensity after electrophoresis.

A d(TCC.CAG.GCT.CAG.ATC.TGG.TC) (-) TAR
d(GAC.CAG.ATC.TGA.GCC.TGG.GA) (+) TAR

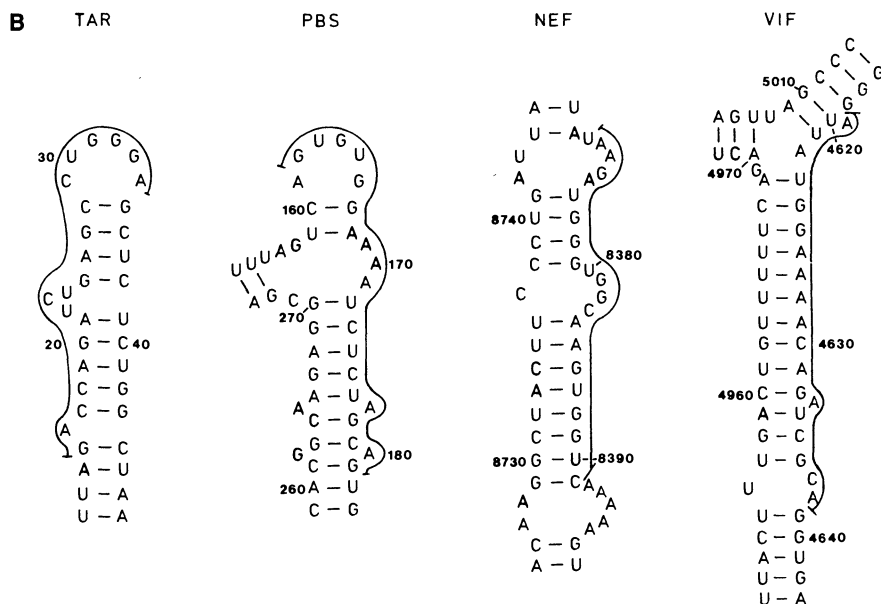
d(CTG.CTA.GAG.ATT.TTC.CAC.AC) (-) PBS
d(GTG.TGG.AAA.ATC.TCT.AGC.AG) (+) PBS

d(GAC.CAC.TTG.CCA.CCC.ATC.TT) (-) NEF
d(AAG.ATG.GGT.GGC.AAG.TGG.TC) (+) NEF

d(TGC.GAT.CTG.TTT.TCC.ATA.AT) (-) VIF
d(ATT.ATG.GAA.AAC.AGA.TCG.CA) (+) VIF

d(AAC.GGC.AGG.CCT.TGC.CAA.AA) RAN

Fig. 3. (A) Selected phosphate-methylated DNAs used for site-specific inhibition of HIV-1. Phosphate-methylated DNA was synthesized according to a three-step procedure (6): (i) base protection with 9-fluorenyl methoxycarbonyl chloride (Fmoc) of an automatically synthesized natural DNA sequence; (ii) methylation of the phosphate groups with *p*-toluenesulfonyl chloride and methanol; and (iii) removal of the Fmoc groups with triethylamine, which preserves the methylated phosphate groups. Purification was performed with preparative thin-layer chromatography. The degree of phosphate methylation is 90 to 100%, as was determined by proton NMR spectroscopy (6), and enzymatic experiments, which show that T₄ polynucleotide kinase is virtually unable to phosphorylate the neutral phosphate-methylated systems. The symbols (-) and (+) denote antisense and sense, respectively (13). Nucleotide numbering is according to (31). TAR is aimed at the loop area of the transactivator responsive region (bases 15 to 34 and 9132 to 9151), which is essential for transcriptional stimulation by the *tat* protein (21). PBS is targeted adjacent to the start site of reverse transcription (bases 162 to 181). NEF and VIF overlap the start codons of the genes for the regulatory protein *nef* (bases 8372 to 8391), and the



infectivity factor *vif* (bases 4619 to 4638), respectively. Control experiments were performed with the RAN sequence, as well as with the natural (phosphodiester) counterparts of the antisense DNAs. (B) Secondary structure of the four target regions by the thermodynamic parameters from Freier *et al.* (32). Structures of minimal free energy were calculated for 1200-nucleotide sections of the HTLV-III_B genome as published by Ratner *et al.* (33).

tion occurs in the TAR target site (C substituted by U at base 29), whereas the PBS target site is identical (Fig. 3B). This is reflected in the inhibitory concentrations, which are similar to HX10 for the PBS constructs, whereas the TAR constructs required five to ten times higher concentrations for inhibition; the RAN showed no inhibitory effect (inhibitory concentration $>3.0 \mu\text{M}$) (20). The RUT virus contains two mutations in the TAR region (G substituted by A at base 32 and C by U at base 23). Correspondingly, no inhibition of syncytium formation was seen for the TAR constructs at up to 10 to 20 times higher concentrations (Table 1).

Our results show that both antisense and sense phosphate-methylated DNA can specifically block the HIV-1 life cycle at low concentration. Since in all HIV-1 strains the TAR region is a functional unit with a hairpin loop and a small variability (21), whereas the PBS sequence displays a much greater diversity with respect to the primary and secondary structure, cytotoxicity studies were performed with the phosphate-methylated TAR constructs. At the inhibitory concentrations for the antisense and sense phosphate-methylated TAR constructs, no cytotoxicity was found (22). When the concentration of the sense phosphate-methylated TAR construct was increased from 0.6 to 6 μM , a linear increase of cytotoxicity to 21% was observed, whereas the antisense phosphate-methylated TAR construct shows a fourfold higher toxicity in the same range (22-24). Therefore, we suggest that the sense phosphate-methylated TAR construct may be an efficient antiviral agent, in particular for chronically infected cells (19).

REFERENCES AND NOTES

- M. L. Stephenson and P. C. Zamecnik, *Proc. Natl. Acad. Sci. U.S.A.* **75**, 285 (1978); G. Zon, *Pharm. Res.* **5**, 539 (1988); C. J. Marcus-Sekura, *Anal. Biochem.* **172**, 289 (1988); A. R. van der Krol, J. N. M. Mol, A. R. Stuitje, *BioTechniques* **6**, 958 (1988).
- In phosphorothioate DNA, the presence of sulfur in the diester linkages entails resistance to nucleases [P. B. Dervan, *Science* **232**, 464 (1986); M. Matsukura *et al.*, *Proc. Natl. Acad. Sci. U.S.A.* **84**, 7706 (1987)]. However, introduction of sulfur in $d(T_{14})$ reduces the duplex \rightleftharpoons coil T_m of a duplex with $d(A_{14})$ from 36° to 20°C , and with poly(rA) from 39° to 20°C (in 0.14M NaCl) [C. A. Stein, C. Subasingha, K. Shinozuka, J. S. Cohen, *Nucleic Acids Res.* **16**, 3209 (1988)]. On the basis of earlier work, we suggest that unfavorable stereoelectronic effects cause a nonhelical conformation around the P-O₃ and P-O₅ bonds (Fig. 1A), which diminishes duplex stability [M. H. P. van Genderen, L. H. Koole, H. M. Buck, *Recl. Trav. Chim. Pays-Bas Belg.* **108**, 28 (1989); M. H. P. van Genderen *et al.*, *Phosphorus Sulfur Relat. Elem.* **32**, 73 (1987)]. Data for the binding properties of phosphoramidate DNA are scarce (3).
- S. Agrawal *et al.*, *Proc. Natl. Acad. Sci. U.S.A.* **85**, 7079 (1988).
- Methyl phosphonate DNA, in which the methyl group is directly bound to phosphorus, is resistant to nuclease breakdown and shows easy diffusion through cell membranes [P. S. Miller, L. T. Braiterman, P. O. P. Ts'o, *Biochemistry* **16**, 1988 (1977)]. However, the solubility in water is low, and a poor hybridization is observed for duplexes over 10 nucleotides long [R. S. Quartin and J. G. Wetmur, *Biochemistry* **28**, 1040 (1989); L. J. Maher III and B. J. Dolnick, *Nucleic Acids Res.* **16**, 3341 (1988)]. The low hybridization strength is due to a nonhelical conformation [K. K. Chacko, K. Lindner, W. Saenger, P. S. Miller, *Nucleic Acids Res.* **11**, 2801 (1983); compare (2)].
- In our initial studies on phosphate-methylated DNA, we observed parallel duplexes based on T-T base pairing (irrespective of phosphorus configuration) (Fig. 1A) [L. H. Koole, M. H. P. van Genderen, H. M. Buck, *J. Am. Chem. Soc.* **109**, 3916 (1987)], and on C-C base pairing (exclusively for the S_p configuration) [L. H. Koole *et al.*, *J. Org. Chem.* **54**, 1657 (1989); P. J. L. M. Quaedflieg *et al.*, *ibid.* **55**, 122 (1990)]. Phosphate-methylated $d(CpG)$ forms a left-handed Z miniduplex (antiparallel), whereas phosphate-methylated $d(GpC)$ is a right-handed B miniduplex (antiparallel) [P. J. L. M. Quaedflieg, L. H. Koole, M. H. P. van Genderen, H. M. Buck, *Recl. Trav. Chim. Pays-Bas Belg.* **108**, 421 (1989)].
- H. M. Moody *et al.*, *Nucleic Acids Res.* **17**, 4769 (1989).
- For methyl phosphotriesters, we found that hybridization with natural DNA and RNA occurs irrespective of the phosphorus configuration (Fig. 1A). Phosphotriesters with more bulky alkyl groups (ethyl and isopropyl) allow hybridization only for the phosphorus configuration where the alkyl substituent is directed away from the helix [M. F. Summers *et al.*, *Nucleic Acids Res.* **14**, 7421 (1986)].
- For the hybrid of phosphate-methylated $d(A_{20})$ with poly(U), formation of a triple helix was detected. Triple helix formation has also been observed for the RNAs poly(A) and poly(U) in high salt solution [W. Saenger, *Principles of Nucleic Acid Structure* (Springer Verlag, New York, 1984); V. I. Lyamichiev *et al.*, *Nature* **339**, 634 (1989)].
- Molecular modeling studies showed that adaptation of phosphate-methylated DNA to the A-geometry results in unfavorable steric interactions between adjacent methylated phosphate groups [M. H. P. van Genderen, L. H. Koole, H. M. Buck, *Proc. K. Ned. Akad. Wet. Ser. B Phys. Sci.* **91**, 53 (1988)].
- A sense phosphate-methylated 22-nucleotide oligomer, complementary to the *lac* operator template strand in *Escherichia coli*, specifically inhibits transcription of the β -galactosidase gene within 20 min [H. M. Moody, S. A. M. Biezen, H. J. M. Kocken, M. H. P. van Genderen, H. M. Buck, *Proc. K. Ned. Akad. Wet. Ser. B Phys. Sci.* **92**, 163 (1989)]. In *Salmonella typhimurium*, two sense phosphate-methylated 21-nucleotide oligomers, differing only by four bases, were targeted on the active-site regions of the alanine racemase genes *alr* and *dadB* (bases 91 to 111 and 94 to 114, respectively). Each phosphate-methylated system exclusively blocks the transcription of its target gene, showing that cross-hybridization involving four mismatches does not occur (20).
- J. E. Ladner *et al.*, *Proc. Natl. Acad. Sci. U.S.A.* **72**, 4414 (1975).
- M. Zuker and P. Stiegler, *Nucleic Acids Res.* **9**, 133 (1981).
- Antisense (-) phosphate-methylated DNA is expected to hybridize with viral (+)RNA, the (+)strand of integrated proviral DNA, and viral mRNA. Sense (+) phosphate-methylated DNA can hybridize with single-stranded proviral (-)DNA and the (-)strand of integrated proviral DNA [W. A. Haseltine, *J. Acquired Immune Defic. Synd.* **1**, 217 (1988)].
- The presence of a loop destabilizes the stem of the hairpin [W. Salsar, *Cold Spring Harbor Symp. Quant. Biol.* **42**, 985 (1977)].
- Four other target sites were reported, for which we have calculated the secondary structure as described (12). Modifications are phosphorothioate (P-S), phosphoramidate (P-N), and methyl phosphonate (P-C). Inhibitory concentrations refer to 100% inhibition of viral infectivity [vide supra (Table 1)]. Three active target sites were reported that contain a hairpin loop (bold) or a loop (italic); $d(\text{GCG}$.
- TAC.TCA.CCA.GTC.GCC.GC) (bases 280 to 299); 3 to 15 μM for P-S and P-N; $d(\text{ACA.CCC.AAT.TCT.GAA.AAT.GG})$ (bases 5349 to 5368); 1.6 to 15 μM for P-S, 3 to 15 μM for P-N (3, 16), and 3 to 17 μM for P-C (17); $d(\text{TCG.TCG.CTG.TCT.CCG.CTT.CTT.CCT.GCC.A})$ (bases 6004 to 6031); 25 μM for P-S with chronically infected cells (19). One target site, $d(\text{CGC.TTA.ATA.CTG.ACG.CTC.TCG.CAC.CCA.T})$ (bases 787 to 814), for which we did not find a hairpin loop, was reported to be significantly less active: $>25 \mu\text{M}$ for P-S (18).
- S. Agrawal *et al.*, *Proc. Natl. Acad. Sci. U.S.A.* **86**, 7790 (1989).
- P. S. Sarin *et al.*, *ibid.* **85**, 7448 (1988).
- M. Matsukura *et al.*, *ibid.* **86**, 4244 (1989).
- Sense phosphorothioate DNA has no effect on viral infectivity (18). Antisense phosphorothioate DNA, targeted at viral mRNA in chronically infected cells, gives a markedly decreased inhibition compared to newly infected cells (16).
- In a model experiment, we were able to show the sensitivity of phosphate-methylated DNA to mismatches. Using phosphate-methylated $d(\text{CAT.GAA.TCC.TAG.CAG.T})$ and its natural complement, we found a T_m of 49°C [ultraviolet (UV) hyperchromicity, DNA concentration of 2 μM], whereas C-T and C-A mismatches at position 8 lower the T_m to 37°C and 25°C , respectively.
- S. Feng and E. C. Holland, *Nature* **334**, 165 (1988).
- Uninfected C81-66 cells (2×10^4 per 100 μl) were incubated 5 days with oligodeoxynucleotides, after which 50 μl of cell suspension was stained with 50 μl of 0.1% trypan blue. Cells that excluded the dye were counted as viable in a hemocytometer, and the percentage reduction of viable cells was determined compared to untreated cells. (-)TAR: 0.6 μM , 9%; 3 μM , 32%; and 6 μM , 89%. (+)TAR: 0.6 μM , 0%; 3 μM , 8%; 6 μM , 21%. Natural (-)TAR: 0.6 μM , 24%; 3 μM , 39%; and 6 μM , 54%. RAN: 6 μM , 0%. The higher toxicity of both antisense TAR constructs is presumably caused by the presence of a TAR homolog elsewhere in the cellular genome.
- Preliminary toxicity experiments in chickens were performed with the antisense phosphate-methylated TAR construct at concentrations up to 20 μM (~90 mg per kilogram of body weight). Over a period of 28 days, no toxic effects (for example, no lethargy and no growth retardation) were observed.
- For the methyl phosphonate 15-nucleotide oligomer $d(\text{CTA.ACC.AGA.GAG.ACC})$, a cytotoxicity of 22% is reported at 22 μM , when only 51% of viral infectivity is blocked (17). For the phosphorothioate 20-nucleotide oligomer $d(\text{CGA.GAT.AAT.GTT.CAC.ACA.AC})$, a cytotoxicity of 67% is found at 15 μM (100% virus inhibition); for the phosphorothioate 15-nucleotide oligomer $d(\text{CTA.ACC.AGA.GAG.ACC})$, the cytotoxicity is 43% at 15 μM (58% virus inhibition) (3).
- J. Goudsmit, J. M. A. Lange, D. A. Paul, G. J. Dadson, *J. Infect. Dis.* **155**, 558 (1987).
- Each reaction mixture of 100 μl contained 0.1 mM of each deoxynucleotide (dNTP), 50 mM KCl, 10 mM tris-HCl (pH 8.3), 0.01% gelatin, 2.5 mM MgCl₂, 100 to 150 ng of each primer, and 1 U of Taq polymerase (Perkin-Elmer Cetus). The primers used to detect cUVD were located 5' and 3' of the HIV-1 long terminal repeat (LTR) in constant domains of the viral genome [5'-LTR $d(\text{ATC.CCG.GGA.TCC.ACC.TCA.GGT.ACC.TTT.AAG.AC})$, including the restriction sites Bam HI and Xma I; 3'-LTR $d(\text{TTG.AAT.TCC.CGA.GTC.CTG.CGT.CGA.GAG.A})$, including the restriction site Eco RI]. Due to the orientation of these primers, only covalently closed cUVD can be amplified. To detect AVD the 5'-LTR primer and a primer located in the U3 region of the HIV-1 LTR were used [internal LTR $d(\text{ATG.GAT.CCA.CAA.GCT.GGT.GTT.CTC.TCC.T})$, including the restriction site Bam HI]. Amplification was performed for 35 cycles (denaturation: 95°C for 1 min; annealing: 55°C for 1 min; and extension: 72°C for 2 min), with a final extension (72°C for 10 min). One-tenth of the samples was separated by electrophoresis in a 1% agarose gel. The specificity of the amplified fragments was determined by Southern (DNA) blot analysis, with HTLV-III_B-LTR containing plasmid as a hybridization probe.

- analysis, with HTLV-III_B-LTR containing plasmid as a hybridization probe.
27. Definitions of nucleic acid conformations according to International Union of Pure and Applied Chemistry—International Union of Biochemistry (IUPAC-IUB) recommendations [*Eur. J. Biochem.* **131**, 9 (1983)]. γ^+ denotes the C₄-C₅ rotamer with O₅ and H₄ antiperiplanar; β^+ is the C₅-O₅ rotamer with phosphorus and C₄ antiperiplanar.
28. Molecular mechanics calculations with the Assisted Model Building and Energy Refinement program (AMBER) have shown that methylated phosphate is easily accommodated in the standard helix geometry, irrespective of the phosphorus configuration, that is, outward methyl orientation (S_p), or location of methyl inside the helix major groove (R_p) [M. H. P. van Genderen, L. H. Koole, O. M. Aagaard, C.

- E. J. van Lare, H. M. Buck, *Biopolymers* **26**, 1447 (1987)].
29. P. J. Hore, *J. Magn. Res.* **55**, 283 (1983); K. Roth, B. J. Kimber, J. Feeney, *ibid.* **41**, 302 (1980).
30. S. Roy and A. G. Redfield, *Biochemistry* **22**, 1386 (1983); A. Heerschap, C. A. G. Haasnoot, C. W. Hilbers, *Nucleic Acids Res.* **10**, 6981 (1982).
31. M. A. Muesing *et al.*, *Nature* **313**, 450 (1985).
32. S. M. Freier *et al.*, *Proc. Natl. Acad. Sci. U.S.A.* **83**, 9373 (1986).
33. L. Ratner *et al.*, *Nature* **313**, 277 (1985).
34. We thank H. M. Moody and J. L. J. van Dongen for the synthesis of phosphate-methylated DNA, and H. J. M. Kocken for performing the T₄ kinase experiments.

10 October 1989; accepted 9 February 1990

Deforestation History of the Eastern Rain Forests of Madagascar from Satellite Images

GLEN M. GREEN AND ROBERT W. SUSSMAN*

Madagascar is biologically one of the richest areas on Earth, and its plants and animals are among the most endangered. Satellite images and vegetation maps based on earlier aerial photographs were used to determine the extent of eastern rain forests in Madagascar and to monitor the rate of deforestation over a 35-year period. In 1985, 3.8 million hectares of rain forest remained, representing only 50 percent of the 7.6 million hectares existing in 1950 and 34 percent of the estimated original extent (11.2 million hectares). Between 1950 and 1985, the rate of deforestation averaged 111,000 hectares per year. Deforestation was most rapid in areas with low topographic relief and high population density. If cutting of forests continues at the same pace, only forests on the steepest slopes will survive the next 35 years.

MADAGASCAR, LOCATED SOME 400 km east of Africa, is the world's fourth largest island, with an area of about 587,000 km². Biologically it is widely regarded as one of the richest areas on Earth containing nearly 8000 endemic species of flowering plants (1–3). Species diversity of both plants and animals is concentrated primarily in the rain forests of eastern Madagascar. This area also has a high species richness per unit area, generally more than in any similar area in Africa (1, 4).

Many plant and animal species are severely threatened (5, 6). Numerous habitats of Madagascar have been degraded since the arrival of humans 1500 to 2000 years ago, and extinctions of species of large mammals and birds have been severe (7, 8). With a current human population of about 11.6 million, a population growth rate of 3.1% per year, and a per capita income of around \$230 per year (9), the major threats to the remaining forest are driven by subsistence

needs and cutting for fuel (10–12). The tropical rain forests of Madagascar before human colonization are thought to have covered much of the eastern coastal plains

and the eastern escarpment of the central plateau that runs along most of the 1600-km length of the island (13, 14). Estimates of the extent of the remaining eastern rain forests have ranged from 2.5 million to 6.9 million ha (100 ha = 1 km²) (3, 10, 12, 15–17), and between 10,000 to 20,000 and 165,000 ha of forest are estimated to have been cleared per year (17, 18). None of these estimates were based on reliable ground or aerial surveys, and each consisted of extrapolations from earlier estimates. Whether the deforestation rate is increasing or decreasing is also uncertain (5, 12).

We have used maps of Humbert and Cours Darne based on aerial photography from 1950 (13) together with satellite image data from 1972 to 1973 and 1984 to 1985 to estimate the area of eastern rain forests of Madagascar and the rate of deforestation over this 35-year period (Fig. 1). Satellite-based remote sensing provides a powerful tool for monitoring deforestation and biodiversity, but it has not been systematically applied globally or in Madagascar (19).

Remotely sensed satellite images at optical wavelengths (0.5 to 1.1 μ m) have been available since 1972 from the Landsat series of satellites (20). Madagascar's eastern rain forests have been successfully distinguished from surrounding savannah and secondary vegetation for limited regions of eastern Madagascar with the use of analog image interpretation applied to Landsat (0.6 to 0.7 μ m, visible red light) images (21, 22). Continuous forest, either primary rain forest or large tracts of closed-canopy secondary forest, is characterized by a dark homogeneous

Table 1. Area of the eastern rain forest of Madagascar, for the period and population density specified.

| Year | Aerial* extent (ha $\times 10^6$) | Forest remain- ing (%) | Forest† perimeter (km $\times 10^3$) | Deforestation rates from 1950 to 1985 (ha $\times 10^3$ /year) |
|--|--|---------------------------------|---|---|
| <i>High (>10 per square kilometer)</i> | | | | |
| Original | 4.7 | 100 | 3.5 | {43} |
| 1950 | 2.4 | 50 | 7.8 | |
| 1985 | 0.89 | 19 | 4.5 | |
| <i>Medium (5 to 10 per square kilometer)</i> | | | | |
| Original | 3.4 | 100 | 2.2 | {37} |
| 1950 | 2.5 | 76 | 4.9 | |
| 1985 | 1.3 | 38 | 5.0 | |
| <i>Low (<5 per square kilometer)</i> | | | | |
| Original | 3.1 | 100 | 3.4 | {31} |
| 1950 | 2.7 | 86 | 5.0 | |
| 1985 | 1.6 | 51 | 6.1 | |
| <i>Total</i> | | | | |
| Original | 11.2 | 100 | 9.1 | {111} |
| 1950 | 7.6 | 67 | 17.7 | |
| 1985 | 3.8 | 34 | 15.6 | |

*A measure of the error in aerial extent at each time period can be estimated by using the number of digitization grid cells (81 ha each) that include forest boundary. The greater the number of these cells, the larger the potential errors. We estimate this error to be $\pm 2\%$, $\pm 6\%$, and $\pm 11\%$, respectively, for original coverage, 1950, and 1985. †Perimeter lengths from 1:1,000,000 scale maps may be underestimated during the digitization process because small-scale features of forest boundaries are lost. We calculate this error to be approximately 10%.

G. M. Green, Department of Earth and Planetary Sciences and the McDonnell Center for the Space Sciences, Washington University, St. Louis, MO 63130.
R. W. Sussman, Department of Anthropology, Washington University, St. Louis, MO 63130.

*To whom correspondence should be addressed.